ACS APPLIED MATERIALS & INTERFACES

Research Article

www.acsami.org

Surface Modifications of Microprojection Arrays for Improved Biomarker Capture in the Skin of Live Mice

Aarshi Bhargav,[†] David A. Muller,[†] Mark A. F. Kendall,[†,‡] and Simon R. Corrie*[,†]

[†]The University of Queensland, Australian Institute for Bioengineering and Nanotechnology, Delivery of Drugs and Genes Group (D^2G^2), St Lucia, QLD 4072, Australia

[‡]The University of Queensland, Diamantina Institute for Cancer, Immunology and Metabolic Medicine, Wooloongabba, QLD, 4102, Australia

Supporting Information

ABSTRACT: New technologies are needed to translate biomarker discovery research into simple, inexpensive, and effective molecular diagnostic assays for use by clinicians or patients to guide and monitor treatment. Microprojection arrays were recently introduced as tools which, when applied to the skin, penetrate into the dermal tissue, and capture specific circulating biomarkers. In our initial work on Microprojection arrays, carbodiimide chemistry was used to immobilize biomarker-specific probes for affinity capture in vivo using a mouse model. However, as the observed capture efficiencies were relatively low, with significant variation across the surface, here we investigated the surface modifications to (a) determine the source of the variability and (b) find ways of improving capture efficiency. We found the protein immobilization step accounted for almost all of the variability in surface uniformity. Varying the protein immobilization conditions following a standard carbodiimide activation process resulted in a reduction in overall variation 14-fold and an increase in captured biomarker amount ~18-fold. In conclusion, we found that investigating and optimizing the surface chemistry of microprojection array devices led to drastic improvements in capturing biomarkers from skin fluid.

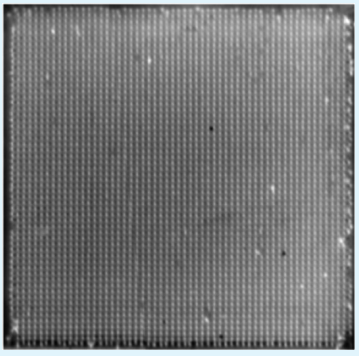

KEYWORDS: *microprojection arrays, microneedles, surface chemistry, EDC, NHS, skin, molecular diagnostics*

INTRODUCTION

The emerging field of rapid molecular diagnosis is expected to lead to earlier disease detection and treatment through frequent, noninvasive patient monitoring at the molecular level.[1,2] However, sampling remains a bottleneck, due in part to the continuing dependence on the needle and syringe. Bulk sampling via needle/syringe collects on the order of ~1−10 mL amounts of nonspecific material, masking the low abundant markers of most interest (e.g., classic plasma proteins 10^6−10^8 pg/mL; tissue leakage products 1×10^3 to 1×10^6 pg/mL; interleukins 1×10 to 1×10^3 pg/mL).[3] Collected samples often require complex laboratory processing (centrifugation, chemical treatments), or the design of complex unit operations in microfluidic chips, prior to assay chemistry and detection. Work in our group is focused on developing alternative "in vivo diagnostic" technologies for selective sampling of biomarkers directly from biological tissues, along with the integration of these methods into traditional or novel chemistry/detection methodologies. A key technology challenge is the design of the substrate surface in contact with native biological fluid, which needs to satisfy requirements of sensitivity, specificity and stability in a complex and uncontrollable environment.

Microprojection Arrays (MPAs) are silicon chips containing an array of cone-like projections (~20 000/cm^2; ~110 μm height used in this study) which, when applied to skin using a spring-loaded applicator, breach the tough corneal layer and penetrate into the underlying dermis.[4−6] Variants of these devices have been applied to solve vaccine or drug delivery challenges,[7−11] but there has only recently been interest in their application as affinity-based capture surfaces. We recently demonstrated selective extraction of a circulating biomarker captured from the skin of live mice using MPAs, using covalent, carbodiimide-mediated probe immobilization onto heterobifunctional PEG layers to limit nonspecific protein adsorption.[12] However, we observed a significantly lower and more variable fluorescent signal across an MPA device surface when applied directly to skin in comparison to serum exposure from the same animals, which in turn may lead to reduced quantitative potential of the technology. Therefore, in this study, we address this issue using a "bottom-up" approach, by investigating the uniformity of the underlying surface chemistry (Scheme 1) and optimizing the probe immobilization chemistry in order to increase target capture efficiency.

For solid-phase assays in which target biomarkers are to be selectively extracted from a biological fluid, antifouling layers and covalent capture probe immobilization strategies are of central importance. Polyethylene glycol (PEG) is a widely used antifouling polymer due to its ease of production or purchase,

Received: January 30, 2012
Accepted: March 9, 2012
Published: March 9, 2012

Scheme 1. Schematics Showing (A) the Surface Modifications Leading to the Indirect ELISA Assays Performed on Mice In vivo; (B) Experimental Design Allowing Analysis of the Interactions between the Different Layers. For Surface Descriptions: (1) = PEG-Au; (2) OVA-PEG-Au; (3) α-OVA-IgG-OVA-PEG-Au

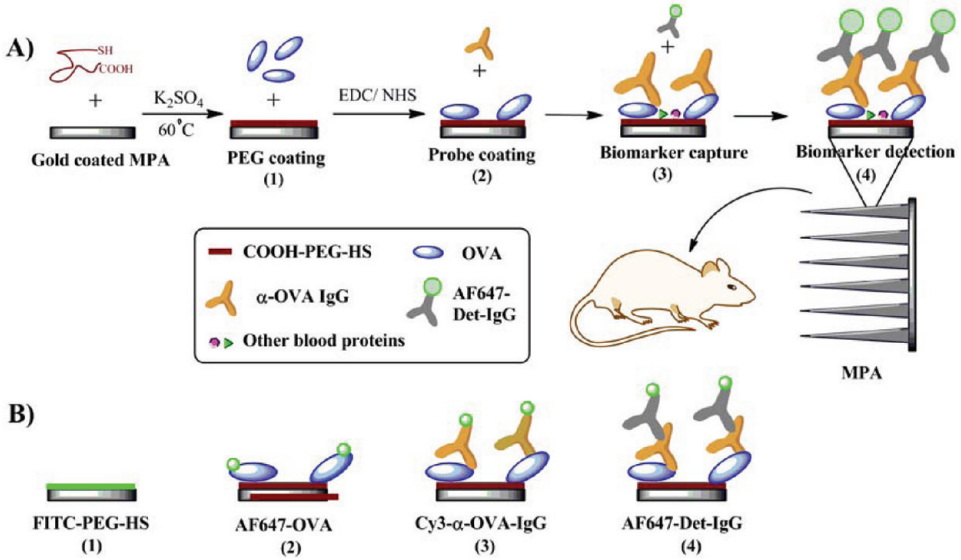

the high surface densities via "cloud-point" grafting,[13] and low protein adsorption characteristics.[14,15] There are a number of other surfaces generating intense interest in the field, including surface-initiated polymerization methods,[16] nonlinear branched ("star") polymers fabricated via a range of methods (e.g., RAFT,[17] ATRP,[18] etc.) and mixtures of polymers to tune protein adsorption.[19] The most widely used immobilization chemistry for this purpose is amide cross-linking chemistry, in which carboxylic acids react with water-soluble carbodiimides (most notably 1-ethyl-3-(3-dimethylaminopropyl) carbodiimide); EDC) in the presence of N-hydroxy succinimide (NHS) to form NHS-activated esters, which react with nucleophiles in solution (in this case, predominantly amines) to form covalent amide bonds. Indeed, there is now sufficient evidence that covalent attachment of these probes onto polystyrene[20] and metal[21−24] surfaces leads to improved probe surface density, orientation, and capture efficiencies in comparison to traditional "passive adsorption". Although straightforward and mild on biological reagents, the yield of immobilized protein is often low because of the complex side reactions that can take place, especially at surfaces,[25] leading to systematically lower surface-active groups available for nucleophilic attack (e.g., formation of anhydrides, which effectively uses two surface carboxyls to form one covalent amide bond and a regenerated but unactivated carboxyl) or negligible surface activation due to the formation of nonreactive urea derivatives.

Sam et al. recently investigated the surface activation step of the EDC/NHS reaction pathway, with the aim of optimizing the surface-active NHS ester yield in preference to the limiting side reactions.[25] Following the progress of the reaction via transmission infrared (ATR) spectroscopy, they found that an equimolar concentration of EDC and NHS reagents resulted in high levels of succinimide in the surface layer, and that only a limited "window" of EDC/NHS concentrations would result in sufficient NHS activation (~5 mM each). In a recent follow-up study,[26] Touahir et al found that the NHS-activation did not go to completion, leaving unreacted carboxylic acid groups able to gain a negative charge at pH > pK_a (i.e., for OVA, pH ~4−6[27,28]). Furthermore, they identified the optimal temperature range to be ~4−20 °C, above which NHS-ester levels decreased. However, recent work has also highlighted that the NHS-activation pathway maybe affected by the composition of the surface underlying the carboxyl groups − Wang et al. recently reported high levels of NHS-activation for PAA surfaces, but negligible NHS-activation under the same conditions for poly(methacrylic acid) (PMAA) surfaces.[29] Although these studies exemplify the contemporary interest in EDC chemistry, there are few studies which have focused on the protein immobilization part of this two-step reaction. Older reports noted the concerning result that in EDC/NHS-mediated immobilization strategies at surfaces, up to 75% or more of the protein is adsorbed to the surface rather than covalently attached;[30,31] to the best of our knowledge, this issue has yet to be investigated more thoroughly.

In this study, we characterized the inherent uniformity across the MPA surface from indirect enzyme-linked immunosorbent assay (ELISA) reactions following in vivo antibody extraction (Scheme 1A/B). We then sought to improve both uniformity and capture efficiency by optimizing the probe immobilization conditions. Finally we investigated the chemical stability of a ^{14}C-labeled protein following application of MPAs to the skin of live mice. This work will be of interest to those designing functional surfaces for in vivo applications, but also to a broader audience interested in optimizing EDC/NHS protein immobilization chemistry.

MATERIALS AND METHODS

Materials. Heterobifunctional polyethylene glycol (referred to as COOH-PEG-SH; 5 kDa) and fluorescently labeled PEG (referred to as FITC-PEG-SH; 3.4 kDa) were purchased from Creative PEGworks (Winston Salem, NC, USA) and Nanocs (Life Research, Burwood East, Victoria, Australia), respectively. 1-Ethyl-3-(3-dimethylaminopropyl) carbodiimide) (EDC) and N-hydroxysuccinimide (NHS) were both purchased from ThermoFisher scientific (Scoresby, Victoria, Australia). 2-(N-morpholino)ethanesulfonic acid (MES) was purchased from MP Biomedicals (Seven Hills, NSW, Australia). The proteins ovalbumin (OVA) and monoclonal antichicken egg albumin (α-OVA-IgG) were obtained from Sigma-Aldrich, and Cy3-labeling of

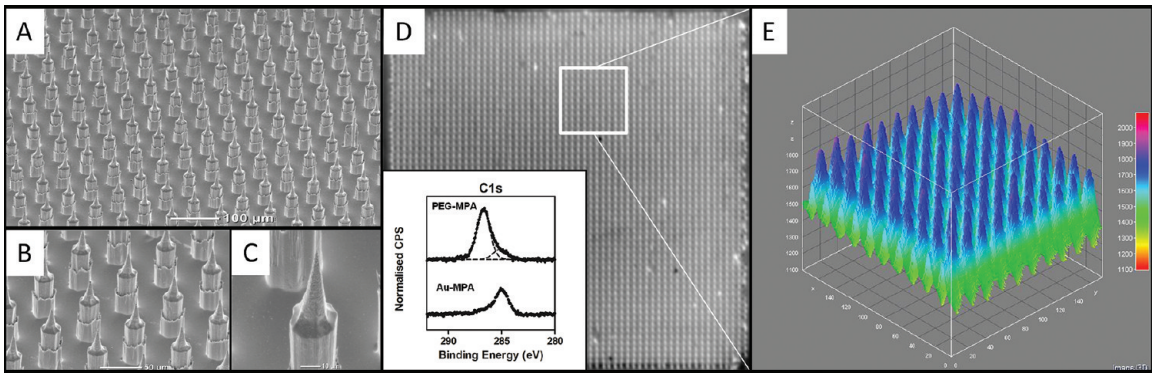

Figure 1. Images of MPA surfaces using (A–C) SEM and (D, E) confocal fluorescence scanning. Inset of D is a high-resolution XPS trace of PEG-modified MPAs in comparison to Au MPAs.

the α-OVA-IgG was performed using a DyLight kit from Thermo-Fisher Scientific (Scoresby, Victoria, Australia). Fluorescently labeled OVA (Alexa Fluor 647, referred to as AF647-OVA and Alexa Fluor 555 conjugates, referred to as AF555-OVA) and Alexa fluor 647-labeled F(ab)2 fragment of goat antimouse IgG (referred to as AF647-Det-IgG) were from Invitrogen (Thornton, NSW, Australia). ^{14}C-OVA was purchased from ARC Radiochemicals (St Louis, MO, USA). All the reagents used for all the experiments were of analytical grade and used without any further purification. Milli-Q water (18 MΩ cm) was used throughout the experiment.

Microprojection Array Preparation and PEG Coating. Gold coated (~100 nm thickness) silicon MPA wafers (silicon; ⟨100⟩), were fabricated in-house using a Deep Reactive Ion Etching (DRIE) process followed by standard chrome/gold evaporation (referred to as Au MPAs).[5] Following thorough rinsing in ethanol, acetone and Milli-Q water for 30 min each, the Au MPAs were cleaned in a preheated base piranha solution (5 mL of 20% ammonia solution in 50 mL of water with 10 mL of 35% w/v hydrogen peroxide) for 15 min at 80 °C to remove organic contaminants, before thorough water cleaning. COOH-PEG-HS or FITC-PEG-HS were coated onto the Au-MPA surface under "cloud-point" conditions (0.2 mg/mL PEG dissolved in 0.6 M K_2SO_4 at 60 °C). A 48-well plate containing three MPAs in each well with 400 μL of coating solution was incubated at 60 °C for approximately 36 h and the resulting MPAs (referred to as PEG-Au MPAs or FITC-PEG-Au MPAs) were washed with 0.6 M K_2SO_4 solution followed by three washes in water to remove excess unbound PEG. These PEG-Au MPAs were analyzed by Scanning Electron Microscopy (SEM; Jeol Neocope JSM-5000) and also X-ray photoelectron spectroscopy (XPS) using a Kratos Axis Ultra as described previously.[12]

Ovalbumin Attachment to PEG-Au MPAs via EDC/NHS Chemistry. PEG-Au MPAs were placed in the well of a 48-well plate containing an equimolar mixture of 5 mM EDC and NHS in 0.1 M MES buffer pH 5 at 200 μL per well. In the "control" conditions, MPAs were incubated at room temperature for 1.5 h with mild agitation after which they were washed with 0.1 M MES in an attempt to remove excess EDC thus avoiding protein polymerization. The MPAs were then suspended in protein solution containing 20 μg/mL of OVA or AF647-OVA in PBS, incubated for 2 h at room temperature with mild agitation and finally rinsed once in 0.1 M glycine for 1 h to cap the unreacted NHS ester. Finally, these OVA-immobilized MPAs (referred to as OVA-PEG-Au MPAs) were washed three times with PBST buffer (PBS containing 0.02% Tween 20 surfactant) to remove unbound proteins.

Indirect ELISA on OVA-PEG-Au MPAs In vitro and In vivo. To generate high titer α-OVA-IgG antibodies in the blood of C57 mice, we injected mice with a saline solution containing 50 μg OVA and 10 μg Quil-A (Sigma; immune adjuvant, added to boost immune response). After 21 days, blood serum of OVA-vaccinated mice (C57BL/6) was obtained by bleeding of the retro-orbital sinuses by trained animal technicians at the AIBN animal facility. After leaving the blood sample at room temperature for two hours to allow sufficient clotting to take place, the sample was centrifuged at 10,000 rpm for five minutes and the supernatant retained as blood serum, stored at −20 °C for long-term storage. Prior to use, each serum sample was confirmed to have sufficient levels of desired antibodies via traditional plate ELISA using a standard method described previously.[4] These verified serum samples were diluted to 10% in PBS and added to the OVA PEG-Au MPAs in each well for 10 min at room temperature. Alternatively OVA PEG-Au MPAs were applied to the flank skin of live anesthetized [ketamine (100 mg/kg) and xylazine (10 mg/kg) in PBS] mice for 10 min with the help of a spring loaded applicator device. The resulting devices (referred to as α-OVA-IgG-OVA-PEG-Au MPAs) were washed thoroughly with PBST to remove any excess proteins from the serum so as to avoid nonspecific binding. A modification to this method was the use of commercially available α-OVA-IgG produced in mice to replace the mouse serum which contains polyclonal antibody and other blood components. The AF647-Det-IgG was used to determine the relative amount of target antibody captured by OVA PEG-Au MPA during the serum or skin incubation. AF647-Det-IgG was prepared as 0.1% in PBS and 200 μL of the solution was added to each well. Following from this, MPAs were incubated for 30 min at room temperature and then washed thoroughly with PBST before analysis via laser scanner. Nanopatches were coated with ovalbumin for quick-release upon application to mice using methods previously described elsewhere.[4] All animal work was performed in accordance with Animal Ethics approval as per regulations of The University of Queensland.

Flat-bed Confocal Laser Scanner. The LS Reloaded Tecan Scanner was used to generate fluorescent images of MPAs coated with fluorophore-labeled molecules. The instrument provided both 532 and 633 nm laser excitation, with emission filters set at 575 and 698 nm, respectively. The 532-line was used for analysis of FITC, Cy3, and AF555 dyes, whereas the 633-line was used for the AF647 dyes used in this study. The MPAs were scanned at a resolution of 4 μm and the photomultiplier gain (PMT) was set to maximize the dynamic range while avoiding saturation of the signal. The resulting images were used for qualitative and quantitative analysis with the help of Image analysis software (Image J). The entire area of the MPA was selected and the mean fluorescence intensity and standard deviation of all the fluorescent pixels in the defined area were measured. Unmodified Au MPAs were used as controls throughout the experiment in laser scanner analysis. The mean fluorescence intensity of the control Au MPAs were considered as background noise and subtracted from the mean fluorescence intensity of the sample to give the final measurements.

Statistical Methods. The data obtained throughout the experiments were summarized using mean values and variability was reported through standard deviation and % CV (coefficient of variation) as specified in the results. Unless otherwise specified, the experiments were repeated in triplicate (three MPAs per treatment). Statistical analysis was performed using ANOVA with Tukey's post test. Nonparametric Kruskal–Wallis test with Dunn's post-test was used when comparing multiple groups of samples from animal

experiments, as it was deemed inappropriate to assume Gaussian error distributions for this data. The acceptance cutoff used to determine statistical significance was $\alpha = 0.05$. Correspondingly, this information is provided in the relevant figures to indicate (**) highly significant (p-value 0.001−0.01), (*) significant (p-value <0.05), and (NS) not significant (p-value >0.05).

RESULTS AND DISCUSSION

Analysis of FITC-PEG-SH Monolayer Uniformity Across a 4 × 4 mm MPA Surface. Figure 1A−C shows a series of SEM and confocal fluorescence images visualizing the geometry of Au MPA devices and individual projections (modeled as cone [35 μm height] plus cylinder [65 μm height]; both with base diameter of 23 μm), from which we can estimate the minimum monolayer uniformity. Upon coating the surface uniformly with a FITC-PEG-SH monolayer, XPS was used to qualitatively confirm successful grafting (Figure 1D, inset). We observed peaks at 285 eV for both FITC-PEG-Au MPAs and Au-MPAs, along with a larger peak at 286 eV for the FITC-PEG-Au MPAs only. The peaks at 285 eV are almost always observed and are likely to be organic contamination, present even after the piranha cleaning treatment. However, the peak at 286 eV is most likely due to the presence of C−O groups present at the surface of the FITC-PEG-Au MPA samples (in agreement with our previous results[12]). A fluorescent scan using a flat-bed confocal scanner showed an "array" style pattern where high intensity "spots" are colocalized with the projections (Figure 1E), clearly due to the higher surface area of these structures relative to a flat area taking up the same footprint. Across an entire PEG-Au MPA surface (Figure 1D) the coefficient of variation (CV, defined as the ratio of standard deviation and mean, expressed as a percentage) of the fluorescent signal was 19.2 ± 1.2% (Table 1). Therefore, to put this variability in context, we can calculate

Table 1. Surface Uniformity Using Control or Optimized OVA Protein Immobilization Conditions

MPA sample (n = 3)	control conditions CV (%)	optimized conditions CV (%)
FITC-PEG-Au	19 ± 2	N/A
AF647-OVA-PEG-Au	533 ± 447	36 ± 8
Cy3-α-OVA-IgG-OVA-PEG-Au	483 ± 18	11 ± 2
A647-Det-IgG-α-OVA-IgG-OVA-PEG-Au	72 ± 34	34 ± 13

the minimum CV for an MPA surface. If the fluorescence intensity of a base pixel is x and ∼10% of the surface of the MPA is covered by projections each with fluorescence intensity of 1.2x (calculated as the average "bright/dark" spots from Figure 1D,E), a 4 μm resolution image of the type shown in Figure 1D has a mean intensity of 1.02x and standard deviation of 0.05x, leading to a minimum CV of 5.3%. This observation suggests that much of the variation in FITC-PEG-Au MPA fluorescent signal can be explained by the presence of the projections, which could easily be normalized based on the repeating geometry.

Specificity of Interactions in a Model Indirect ELISA System. The experimental design outlined in Scheme 1B was carried out to investigate the nature of the OVA-PEG interaction in the presence or absence of EDC/NHS and also to investigate the subsequent affinity interactions in the model indirect ELISA system. Because of previous reports suggesting that much of the immobilized protein remaining after EDC/NHS chemistry is not covalently attached but adsorbed,[30,31] we investigated the degree of sequential, batch-wise washing steps required to remove as much of this material as possible. Figure S1 in the Supporting Information shows that 15 washing steps were generally required, beyond which no reduction in adsorption was observed. This process was used for all experiments conducted in this study and controls without EDC/NHS activation have been included throughout.

First, we observed significant nonspecific binding of AF647-OVA, Cy3-α-OVA-IgG and AF647-Det-IgG to bare Au MPAs (Figure 2A-C). This was expected because Au surfaces can interact with the amino acid side chains of proteins via hydrophobic interactions or chemisorption with certain functional groups (e.g., −SH, $-NH_2$). This is a clear disadvantage of the Au surface for this purpose as even with an antifouling layer in place any defects or contaminants present prior to layer formation may present favorable nucleation sites for nonspecific adsorption in subsequent assay steps. However, the addition of a PEG layer (5 kDa; ∼0.6 PEG/nm^2) resulted in a decrease in signal of 89, 98, and 99% for AF647-OVA, Cy3-α-OVA-IgG, and AF647-Det-IgG, respectively, likely because of the antifouling effect of PEG. Also, by comparing the adsorption of AF647-OVA on PEG-Au MPAs in the presence or absence of EDC/NHS activation, it appears that under control conditions used in this study, ∼ 20% of the OVA coated onto the MPAs is due to adsorption alone (Figure 2A).

Second, Cy3-α-OVA-IgG specifically bound to OVA-PEG-Au MPAs with ∼30-fold higher binding than PEG-Au MPAs alone (Figure 2B). Although capture of the biomarker in a protein-free buffered solution allowed us to confirm the specific affinity interaction, it is an artificial solution that does not allow for the competitive effects of nonspecific protein adsorption at the interface. This is especially important for MPA technology development, because the surface needs to operate in natural biological fluids in vivo. Therefore we diluted the Cy3-α-OVA-IgG in PBST containing 10% normal mouse serum to introduce the protein component of a real biological fluid without significantly affecting pH or ionic strength, both of which would likely also affect capture and fluorescent signal. As expected, we observed that the Cy3-α-OVA-IgG capture was significantly reduced with the addition of serum, indicating that the extra protein component inhibits specific interaction between OVA and the target biomarker (Figure 2B). Finally, AF647-Det-IgG specifically bound to α-OVA-IgG-OVA-PEG-Au MPAs with or without serum present (Figure 2C). Interestingly, this is the only specific interaction that resulted in a significantly higher fluorescent signal in comparison to adsorption to Au MPAs. This could be explained by the signal amplifying nature of the antibodies, as multiple AF647-Det-IgG molecules can bind to each target antibody.

Improved Protein Immobilization Conditions for Increased Target Antibody Capture. Results in Table 1 suggest that the protein immobilization procedure accounted for a significant variation in signal intensity across the MPA surface. In order to address this issue, we varied the conditions of the protein immobilization step in the EDC/NHS chemistry while using the activation conditions elegantly defined in recent works by Touahir and Sam et al.[25,26] In a three-factor, three-level factorial design, we varied pH (4.5, 7.4, 8.5), time (t; 30, 120, 960 min) and temperature (T; 4, 24, or 37 °C), assessing the response by measuring the degree of AF647-OVA bound with triplicate replication. The combination of "medium" levels

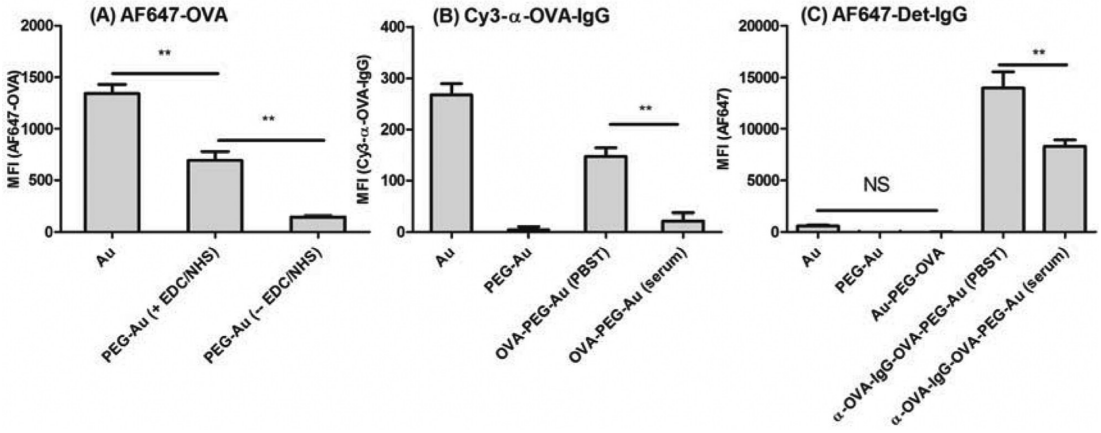

Figure 2. Bar charts showing the fluorescence intensities of different species interacting with MPA surfaces using control protein coupling conditions. (A) Surfaces interacting with AF647-labeled OVA; (B) surfaces interacting with Cy3-α-OVA-IgG, and (C) surfaces interacting with AF647-Det-IgG. Note that ** indicates p-value <0.01, * indicates p-value <0.05 and NS indicates p-value >0.05.

for each factor represented the "control" conditions used in this study. To identify the set of conditions which promoted the highest degree of covalent OVA protein immobilization, the average signal of three MPAs exposed to OVA under the same conditions but without activation was subtracted for each data point. ANOVA clearly showed that all three factors, along with their respective interactions, had significant effects on OVA immobilization. Pairwise multiple comparison tests showed that pH = 4.5, T = 37 °C, and t = 960 min (p < 0.001 in each case) were the optimal levels within each factor. However, from analysis of the interactions, the positive effects of low pH (p < 0.001) and higher T (p < 0.001) were only significant over the longest reaction time. Indeed, the optimal combination of factors (pH 4.5, T = 37 °C, t = 960 min; herein referred to as "optimized conditions") resulted in ∼60-fold increase in fluorescent signal. Furthermore, the degree of uniformity across the MPA surfaces also improved with respect to the control (Table 1), possibly because of the increase in signal.

The effect of pH on OVA coupling to PEG-Au surfaces can be explained in the context of charge and pK_a of both the surface and protein. The isoeletric point (pI) of OVA is ∼4.9 and Pei et al.[32] showed that carboxylated PEG surfaces have a pK_a ∼ 5, below which the surface rapidly loses its negative charge. When pH 4.5 is used in the protein coupling step, OVA carries an overall positive charge (pH < pK_a) and the surface covers a negative overall charge, because of the presence of at least some unprotonated carboxylic acids.[25] This situation may encourage electrostatic attraction, in turn facilitating covalent bond formation, and nucleophilic attack of the protonated amine onto the NHS ester occurs.[25,32] Importantly, this electrostatic adsorption may also favor adsorption alone, however in this study we accounted for this effect under all conditions. However, when using pH >5 (i.e., including the control conditions), OVA carries a net negative charge (pH > pK_a) and the surface also carries a net negative charge due to the presence of carboxylate anions (pH > pK_a) remaining due to less than 100% EDC/NHS activation. Therefore, electrostatic repulsion between the negatively charged surface and protein may be the reason for poor OVA grafting at the more neutral or slightly basic pH conditions, as seen for other systems.

Demonstration of Target Capture and Stability of Coating in Mouse Skin. Following analysis of the indirect ELISA chemistry and improvements in surface coating uniformity and α-OVA-IgG capture efficiency, we moved on to investigate the capture efficiency in vivo and the stability of the OVA attachment chemistry in the mouse. For measuring capture efficiency in vivo, we applied OVA-PEG-Au MPAs to the mouse flank, as we have found higher biomarker extraction levels at this site in comparison to the ear (manuscript in preparation). Figure 3A shows the results from the indirect ELISA performed by applying the OVA-PEG-Au MPAs to the flank skin of live mice followed by subsequent AF647-Det-IgG binding and fluorescence analysis. For capture either in vivo or in vitro (serum from same animals diluted 10% in PBST) the optimized protein coupling conditions yielded significantly higher AF647-Det-IgG signals in vaccinated mice with respect to controls, 18-fold and 140-fold higher respectively. In the case of the control protein immobilization conditions, higher antibody capture was also observed for the vaccinated animals in comparison to controls, however the signal/noise ratios were far lower (∼2.5-fold for both in vitro and in vivo). Regardless of immobilization conditions, capture efficiency was lower in vivo in comparison to in vitro, likely due to poor mass transfer in the biological fluid in comparison to the in vitro buffer system. Serum IgG levels of mice were confirmed via traditional plate ELISA assay; see Figure S2 in the Supporting Information.

To test the stability of the surface coating used in these studies in vivo (in terms of amount of probe released into the skin), we measured the absolute amount of ^{14}C-OVA released into excised ears following EDC/NHS immobilization chemistry, with respect to unused control OVA-PEG-Au MPAs. Importantly, the unused control devices allowed us to compare the absolute OVA surface density as a function of OVA immobilization conditions. In the case of the optimized conditions, the surface density of ∼3.2 × 10^{-5} OVA/nm^2 is significantly less than a full monolayer, which is ∼0.03−0.04 OVA/nm^2 (assuming OVA protein is a rod structure with dimensions 7 × 5 × 4.5 nm^3). In comparison, the control protein coupling conditions yielded background signals in the scintillation counter (i.e., < 4.4 × 10^{-7} OVA/nm^2). In terms of stability, we could not estimate the amount of ^{14}C-OVA released into the mouse skin for the control protein coupling conditions, as the signals were all at background levels. For the optimized protein coupling conditions, approximately 75% of ^{14}C-OVA was retained on the OVA-PEG-Au MPAs after the 10

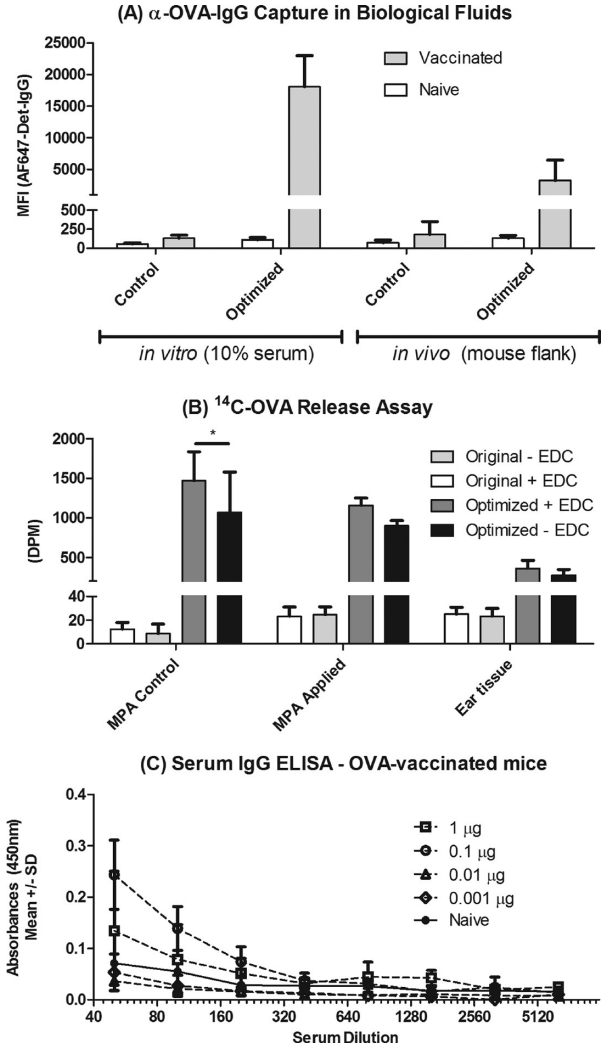

Figure 3. Charts showing the fluorescence intensities of different species interacting with OVA-PEG-Au MPA surfaces. (A) Surfaces interacting with AF647-labeled OVA; (B) radio-labeled ^{14}C-OVA release into skin as a function of surface chemistry; (C) serum IgG antibody response to nanopatch-delivered OVA in a titration covering 0.0001 − 1 μg OVA. Note that ** indicates p-value <0.01, * indicates p-value <0.05 and NS indicates p-value >0.05.

min incubation, leaving ∼16 pg deposited into the skin. The presence or absence of EDC/NHS activation did not alter the percent retained (although in the case of adsorbed OVA, less overall protein remained on PEG-Au MPAs following immobilization and washing). This suggests that in the case of adsorbed protein, for the time period used in this experiment, covalent attachment of OVA did not improve the stability of the coating in the mouse skin. To investigate the effect of releasing pg amounts into the skin, we immunized mice with OVA (1−0.001 μg) via nanopatch delivery to the skin, focusing at the same site of application as for the extraction experiments. As shown in Figure 3C, while releasing 0.1−1 μg OVA invoked an IgG response above that of unimmunized animals, 0.01−0.001 μg yielded negligible responses (less than unimmunized animals), suggesting that delivery of OVA in amounts <10 ng does not elicit a systemic response. Importantly, further investigation into local skin responses (e.g., local wound healing, hypersensitivity responses, etc.) is required to investigate effects of probe release in the skin more fully. However, to our knowledge, this is the first time that the stability of an amide-mediated coupling strategy has been investigated in vivo.

CONCLUSIONS

In this work, we show the first investigation of the surface chemistry underlying MPA-based biochemical assays, finding that optimization of protein immobilization conditions significantly improved antibody capture from the skin of live mice. These results have broader implications, and are conceptually applicable to any situation in which increasing protein immobilization on a surface using EDC/NHS chemistry is desired. We also investigated the stability of this chemistry in vivo, finding that ∼20% of the protein was released into the skin upon application. This raises a significant issue for developers of implantable devices, as some of the released material may provoke toxic or immune responses. We will now focus on investigating the mechanisms linking nonspecific protein in serum to poor capture efficiency in order to inform investigations into novel antifouling layers. Furthermore, we will also try to increase capture efficiency, and hence assay sensitivity, by focusing on the biology of the skin, and the mechanisms available to enhance local mass transfer.

ASSOCIATED CONTENT

Supporting Information

Supplementary Figures S1 and S2. This material is available free of charge via the Internet at http://pubs.acs.org/.

AUTHOR INFORMATION

Corresponding Author

*E-mail: s.corrie1@uq.edu.au. Tel: +617 3346 4209. Fax: +617 3346 3973.

Notes

The authors declare the following competing financial interest(s):Note: Authors SC and MK are inventors on a patent that has recently been licensed to Vaxxas, Pty, Ltd. MK is a co-founder and Chief Technical Officer; SC is employed only by The University of Queensland.

ACKNOWLEDGMENTS

We acknowledge funding from the Australian Research Council (ARC Discovery DP0985502; ARC Future Fellowship (MAFK)), the Queensland Government (QLD Smart Futures Postdoctoral Fellowship (SRC)). We also acknowledge the facilities, and the scientific and technical assistance, of the Australian National Fabrication Facility (ANFF Queensland Node), the Australian Microscopy & Microanalysis Research Facility (AMMRF) at the Centre for Microscopy and Microanalysis (CMM) and the AIBN Animal House run by the University of Queensland Biological Resources group, all located at The University of Queensland. For technical support we thank Ms Sally Yukiko for Nanopatch preparation.

REFERENCES

(1) Etzioni, R.; Urban, N.; Ramsey, S.; McIntosh, M.; Schwartz, S.; Reid, B.; Radich, J.; Anderson, G.; Hartwell, L. *Na. Rev. Cancer* **2003**, *3*, 243−252.
(2) Mabey, D.; Peeling, R. W.; Ustianowski, A.; Perkins, M. D. *Nat. Rev. Microbiol.* **2004**, *2*, 231−240.
(3) Anderson, N. L. *Clin. Chem.* **2010**, *56*, 177−185.
(4) Crichton, M. L.; Ansaldo, A.; Chen, X.; Prow, T. W.; Fernando, G. J. P.; Kendall, M. A. F. *Biomaterials* **2010**, *31*, 4562−4572.

(5) Jenkins, D.; Corrie, S.; Flaim, C.; Kendall, M. A. F. *RSC Advances* **2012**, DOI: 10.1039/c2ra20153d.
(6) Crichton, M. L.; Donose, B. C.; Chen, X.; Raphael, A. P.; Huang, H.; Kendall, M. *Biomaterials* **2011**, *32*, 4670−4681.
(7) Fernando, G. J. P.; Chen, X. F.; Prow, T. W.; Crichton, M. L.; Fairmaid, E. J.; Roberts, M. S.; Frazer, I. H.; Brown, L. E.; Kendall, M. A. F. *Plos One* **2010**, *5*, 11.
(8) Chen, X. F.; Kask, A. S.; Crichton, M. L.; McNeilly, C.; Yukiko, S.; Dong, L. C.; Marshak, J. O.; Jarrahian, C.; Fernando, G. J. P.; Chen, D. X.; Koelle, D. M.; Kendall, M. A. F. *J. Controlled Release* **2010**, *148*, 327−333.
(9) Corbett, H. J.; Fernando, G. J. P.; Chen, X.; Frazer, I. H.; Kendall, M. A. F. *Plos One* **2010**, *5*, e13460.
(10) Kask, A. S.; Chen, X. F.; Marshak, J. O.; Dong, L. C.; Saracino, M.; Chen, D.; Jarrahian, C.; Kendall, M. A.; Koelle, D. M. *Vaccine* **2010**, *28*, 7483−7491.
(11) Prow, T. W.; Chen, X.; Prow, N. A.; Fernando, G. J. P.; Tan, C. S. E.; Raphael, A. P.; Chang, D.; Ruutu, M. P.; Jenkins, D. W. K.; Pyke, A.; Crichton, M. L.; Raphaelli, K.; Goh, L. Y. H.; Frazer, I. H.; Roberts, M. S.; Gardner, J.; Khromykh, A. A.; Suhrbier, A.; Hall, R. A.; Kendall, M. A. F. *Small* **2010**, *6*, 1776−1784.
(12) Corrie, S. R.; Fernando, G. J. P.; Crichton, M. L.; Brunck, M. E. G.; Anderson, C. D.; Kendall, M. A. F. *Lab Chip* **2010**, *10*, 2655−2658.
(13) Kingshott, P.; Thissen, H.; Griesser, H. J. *Biomaterials* **2002**, *23*, 2043−2056.
(14) Unsworth, L. D.; Tun, Z.; Sheardown, H.; Brash, J. L. *J. Colloid Interface Sci.* **2005**, *281*, 112−121.
(15) Unsworth, L. D.; Sheardown, H.; Brash, J. L. *Biomaterials* **2005**, *26*, 5927−5933.
(16) Hucknall, A.; Rangarajan, S.; Chilkoti, A. *Adv. Mater. (Weinheim, Ger.)* **2009**, *21*, 2441−2446.
(17) Luzon, M.; Boyer, C.; Peinado, C.; Corrales, T.; Whittaker, M.; Tao, L.; Davis, T. P. *J. Polym. Sci., Part A: Polym. Chem.* **2010**, *48*, 2783−2792.
(18) Feng, W.; Zhu, S. P.; Ishihara, K.; Brash, J. L. *Langmuir* **2005**, *21*, 5980−5987.
(19) Nagasaki, Y. *Polym. J. (Tokyo, Jpn.)* **2011**, *43*, 949−958.
(20) Bora, U.; Chugh, L.; Nahar, P. *J. Immunol. Methods* **2002**, *268*, 171−177.
(21) Vashist, S. K.; Dixit, C. K.; MacCraith, B. D.; O'Kennedy, R. *Analyst (Cambridge, U. K.)* **2011**, *136*, 4431−4436.
(22) Thebault, P.; Boujday, S.; Senechal, H.; Pradier, C.-M. *J. Phys. Chem. B* **2010**, *114*, 10612−10619.
(23) Tajima, N.; Takai, M.; Ishihara, K. *Anal. Chem.* **2011**, *83*, 1969−1976.
(24) Caruso, F.; Rodda, E.; Furlong, D. N. *J. Colloid Interface Sci.* **1996**, *178*, 104−115.
(25) Sam, S.; Touahir, L.; Andresa, J. S.; Allongue, P.; Chazalviel, J. N.; Gouget-Laemmel, A. C.; de Villeneuve, C. H.; Moraillon, A.; Ozanam, F.; Gabouze, N.; Djebbar, S. *Langmuir* **2010**, *26*, 809−814.
(26) Touahir, L.; Chazalviel, J. N.; Sam, S.; Moraillon, A.; de Villeneuve, C. H.; Allongue, P.; Ozanam, F.; Gouget-Laemmel, A. C. *J. Phys. Chem. C* **2011**, *115*, 6782−6787.
(27) Guo, X.; Yan, H.; Guo, R. *Chin. J. Chem.* **2008**, *26*, 1589−1595.
(28) Smith, E. R. B. *J. Biol. Chem.* **1936**, *113*, 473−478.
(29) Wang, C.; Yan, Q.; Liu, H.-B.; Zhou, X.-H.; Xiao, S.-J. *Langmuir* **2011**, *27*, 12058−12068.
(30) Smith, A. M.; Ducey, M. W.; Meyerhoff, M. E. *Biosens. Bioelectron.* **2000**, *15*, 183−192.
(31) Tyagi, R.; Roy, I.; Agarwal, R.; Gupta, M. N. *Biotechnol. Appl. Biochem.* **1998**, *28*, 201−206.
(32) Pei, Z.; Anderson, H.; Myrskog, A.; Duner, G.; Ingermasson, B.; Aastrup, T. *Anal. Biochem.* **2010**, *398*, 161−168.